IMPACT OF HIGH TEMPERATURE AND PRESSURE TO STEEL PASSIVATION IN CO₂ ATMOSPHERE

3 Mojca Slemnik¹

- 4 University of Maribor, Faculty of Chemistry and Chemical Engineering, Smetanova 17, 2000
- Maribor, Slovenia 5

Abstract

1

2

6

7

8

9

10

11

12

13

14

The corrosion behaviour of AISI 347 in 0.1 M sulphuric acid at elevated temperature and pressure up to 300 bar in a CO₂ atmosphere was investigated by surface analysis and electrochemical methods. Corrosion reactions in which CO₂ is present accelerate the formation of a protective FeCO₃ layer, but the success of such a passivation depends on the saturation concentration and the corresponding temperature. Not nearly the same, but even better results were obtained at lower temperatures by increasing the pressure. In order to explain the differences in corrosion rate between the samples, the activation energy for the layer dissolution was also discussed. Presumably it is the effect of compression by the CO₂ on the iron carbonate film that leads to its porosity properties and thus to its corrosive behaviour.

15 16

17

Key words: stainless steel, EIS, CO₂ corrosion, high pressure

18

20

21

22

23

24

25

26

27

28

1. Introduction 19

The steel AISI 347 is generally used in extreme conditions, e.g. aggressive media, at high temperatures and/or high pressures, mostly in pipeline systems, in the gas industry, especially for industrial gas cylinders, etc. It belongs to the group of steels with the low carbon content, which can be additionally protected with inhibitors or coatings. The niobium content improves the mechanical properties of the steel by increasing hardness and the corrosion properties by reducing pitting.² It has a great affinity to carbon, which precipitates as a carbide. Niobium carbides are more stable than those of chromium, they remove carbon from the solid solution and stabilize the steel.³ Niobium also promotes the formation of chromium oxides and accelerates the formation of an iron oxide enriched passive layer in the outer layer and

chromium, manganese and iron oxides in the inner layer at high temperature. 4 Carbon dioxide is useful as a supercritical fluid in several chemical processes as it changes its properties such as density, diffusivity, viscosity, compressibility, and surface tension by changing temperature and/or pressure. When it is used in a corrosive environment, it changes its parameters such as pH, partial pressure, temperature, concentration, compressibility etc. and influences the formation of a protective passive layer on the surface of the metal and thus its protective properties. To reduce the corrosion rate, some authors suggest different coatings, prepassivation 5-8 or the use of efficient inhibitors 9-11 for steel in CO2 and also aggressive environments. Not many CO₂ corrosion studies have been carried out on low carbon steels, ¹² but the fact is that steel exposed to the CO₂ environment triggers a spontaneous passivation process as it causes the formation of the FeCO₃ layer that protects the metal surface and reduces the corrosion rate. Dugstad ¹³⁻¹⁵ explains how the term CO₂ corrosion covers a wide range of electrochemical mechanisms and complex processes. The interaction between protective FeCO₃ layer formation, corrosion rate and iron ion concentration in water was described in detail. CO₂ corrosion reactions are divided into anodic and cathodic processes. In principle, corrosion 44 reactions in CO₂ create a chemical environment that accelerates the formation of iron carbonate, which is often oxidized in air. 16 Such a layer is formed by the precipitation of iron carbonate when its saturation concentration is exceeded. 17, 18 The concentrations of iron and carbonate ions must locally exceed the solubility limit. The precipitation rate is low at low temperatures, so that in this case a very small amount of layer is formed and a higher temperature is required for process efficiency. If the rate of iron and carbon precipitation is equal to or higher than the corrosion rate, a dense protective layer is formed, but if the corrosion process is faster, the layer becomes porous and unprotective. 19 Therefore, special attention has been paid to the study of iron carbonate solubility under different conditions. W. Sun and S. Nešić²⁰ developed a uniform 54 equation for iron carbonate solubility that is valid for a wide range of parameters and is based on literature data. In the case of CO₂ corrosion, however, many effects must be taken into account.²¹ As expected, the temperature increases the corrosion rate, especially at low pH values, when no precipitation of iron carbonate can occur. On the other hand, the solubility of 58 iron carbonate increases with rising temperature, and when it finally exceeds the solubility limit of iron carbonate, its protective scale formation reduces the rate of corrosion. In addition to temperature and many other effects, the effect of the CO₂ partial pressure was also investigated. 22 Y. Sun and S. Nešić 23 studied an increase in P_{CO2} from 3 to 20 bar and concluded, that P_{CO2} generally leads to an increase in the corrosion rate due to an increased concentration of H₂CO₃, which further accelerates the cathodic reaction and thus the corrosion rate. However, when the

29

30

31

32

33

34

35

36

37

38

39

40

41

42

43

45

46

47

48

49

50

51

52

53

55

56

57

59

60

61

62

conditions for the formation of iron carbonate are favourable, a higher P_{CO2} value increases the carbonate ion concentration, which further leads to higher supersaturation and scale precipitation.²⁴ Y. Zhang et al.²⁵ studied CO₂ corrosion behaviour between low partial pressure (1 MPa) and supercritical conditions (9.5 MPa) at various temperatures (from 50 to 130°C) and immersion times. It was concluded that the change in partial pressure does not alter the corrosion mechanism, but only affects the corrosion rate, so that the rate is higher under supercritical conditions. X. Li et al.²⁶ investigated the nature of corrosion scales in extremely aggressive environments at high temperature and CO₂ high pressure and found that the corrosion resistance performance of corrosion scales decreases with increasing temperature and CO₂ pressure, finding the decreasing pitting and repassivation potential with increasing density and diffusivity of the acceptor in the scales. Z.M. Wang et al.²⁷ succeeded in the *in situ* observation of the CO₂ corrosion process under high pressure from active dissolution, the formation of a defective corrosion layer up to local layer dissolution and pitting.

In general, corrosion protection methods include the use of corrosion resistant materials, coatings, corrosion inhibitors, electrochemical protection, rust preventing oils or greases and surface treatments.²⁸ The most natural and spontaneous phenomenon in the surface treatment of metals is passivation process, which can also be accelerated with a suitable approach. In our previous study we worked on improving the surface passivation at 25°C by forming a stable protective layer of iron carbonate by exposing the system only to elevated pressures of up to 300 bar²⁹ in acidic environment. In the following we were interested in the corrosion behaviour of steel in sulphuric acid at elevated pressures up to 300 bar and simultaneously elevated temperatures of 50 and 75°C. We also investigated the temperature dependence and the values of the activation energies required for the dissolution process of protective layer.

2. Experimental

2.1. Material and sample preparation

Stainless steel AISI 347 made in Železarna Ravne, Slovenia, has been investigated, with following chemical composition in wt%: Fe 69.882 %, C 0.05 %, Si 0.53 %, Mn 1.32 %, P 0.024 %, S 0.024 %, Cr 17.95 %, Ni 9.66 % in Nb 0.56 %.

Samples were mechanically polished with 400 - 1200 grit abrasive paper, polished with diamond pastes to a mirror – like quality, and degreased in acetone, p.a. (Fluka).

97	The high pressure experiments were performed in a thermostated autoclave with 65 mL volume,
98	which is designed for a maximum temperature of 200°C and pressure to 400 bar. The
99	temperature was kept constant with the outdoor thermostat Lauda RC6 CP and measured with
100	the Greisinger thermometer GMH 3230 with an accuracy of \pm 0.1°C. For the evacuation of the
101	autoclave the vacuum pump with a provided underpressure of 3.45 Pa was used. CO2 was dosed
102	into the autoclave with the pump PM101. The pressure was measured with the sensor Wika (PI)
103	with an accuracy of 0.01 MPa.
104	The samples were immersed in 40 mL of 0.1 M H ₂ SO ₄ , which was prepared from 96 % acid,
105	p.a. (Carlo Erba), previously blown trough with CO ₂ for 10 minutes with a purity of 99.995 %
106	(Messer Slovenija). The autoclave was evacuated and filled with CO ₂ to the desired pressure.
107	The solution was stirred for 1 hour with a magnetic stirrer at a frequency of 800 min ⁻¹ .
108	After pressure relief, the samples, which were already covered with the resulting
109	layer, were analysed with the Sirion 400 NC (SEM - Scanning Electron Microscopy) and EDS
110	(Energy Dispersive Spectroscopy) INCA 350 analysers.
111	
112	2.2. Electrochemical tests
113	
114	The electrochemical measurements were performed in a standard three-electrode cell with
115	sample as working electrode, a platinum counter electrode and SCE reference. The cell was
116	filled with 300 ml 0.1 M sulfuric acid. The data were collected with Electrochemical Interface
117	Solartron1287 and Frequency Response Analyzer Solartron 1250.
118	The samples were polarised at OCP until the system reached stability and then the
119	impedance curves were recorded in the frequency range between 60 kHz and 1 mHz. The
120	amplitude of the excitation voltage was 10 mV.
121	Potentiodynamic curves from 0.6 V to 1.0 VSCE were recorded at a sampling rate of 1 mVs ⁻¹ .
122	All data were acquired and processed with the ZPlot, ZView, CorrWare and CorrView
123	instruments developed by Scribner Associates, Inc. ³⁰
124	
125	
126	

3. Results and discussion

3.1. Surface analysis

It is generally known that during CO₂ corrosion of steel the system first leads to the formation of H_2CO_3 and further to the formation of $FeCO_3$ (siderite): $^{25,\,31}$

$$CO_{2} + H_{2}O \rightarrow H_{2}CO_{3}$$

$$2H_{2}CO_{3} + 2e^{-} \rightarrow H_{2} + 2HCO_{3}^{-}$$

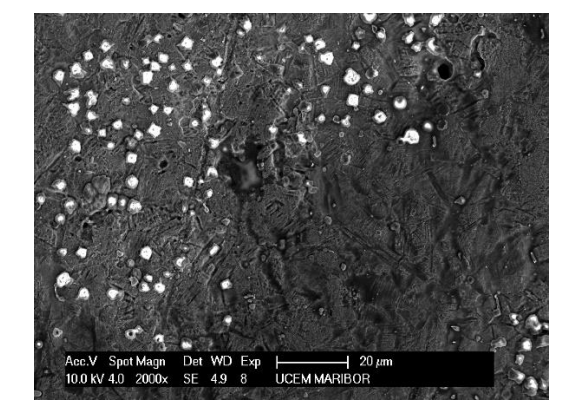
$$133 \quad HCO_{3}^{-} \rightarrow H^{+} + CO_{3}^{2-}$$

$$Fe \rightarrow Fe^{2+} + 2e^{-}$$

$$Fe^{2+} + CO_{3}^{2-} \rightarrow FeCO_{3}$$

$$(1)$$

Layer growth is caused by precipitation after exceeding the saturation concentration under suitable conditions. Our samples, which were exposed to CO₂ in a closed autoclave system under different pressure and temperature values, were covered with a layer whose morphology was further investigated with SEM and EDS.



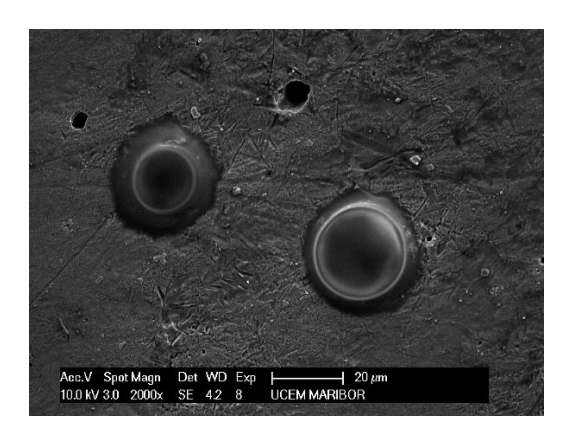
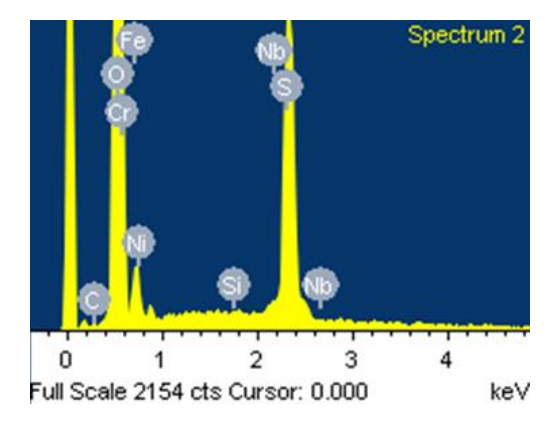


Figure 1. SEM images for AISI 347 at 50°C and pressure a) 100 bar, b) 300 bar.



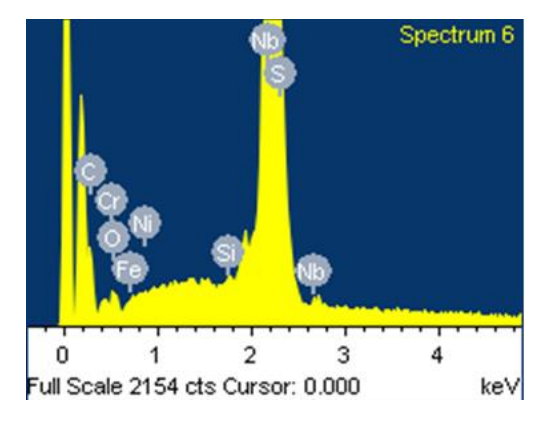
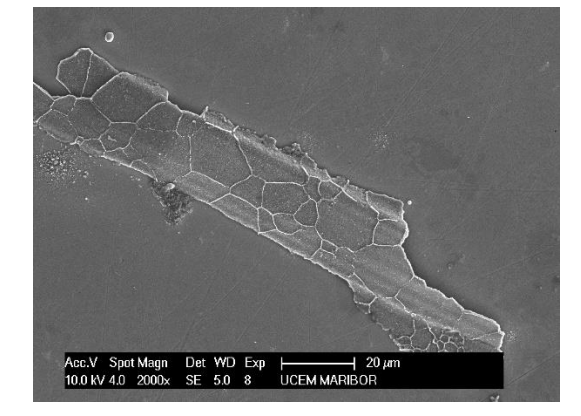


Figure 2. EDS results for AISI 347 from Figure 1a): a) white precipitants and b) dark area.

White spots (Figure 1a and Figure 2a) were detected as precipitants with a high oxygen content (43%) in a 3:1 ratio with iron (16%), which clearly indicates the formation of FeCO₃, while at the same time a high chromium content (20%) was detected. Dark precipitants (Figure 2b) indicate a high content of niobium (91%). The sample treated at 300 bar (Figure 1b) shows large particles with a high content of oxygen (43%), iron (16%) and some chromium (13%). Some large pits (pitting corrosion) are also visible in the dark area. It was found,³² that the FeCO₃ layer on the steel surface grows even in pits of locally corroded samples.



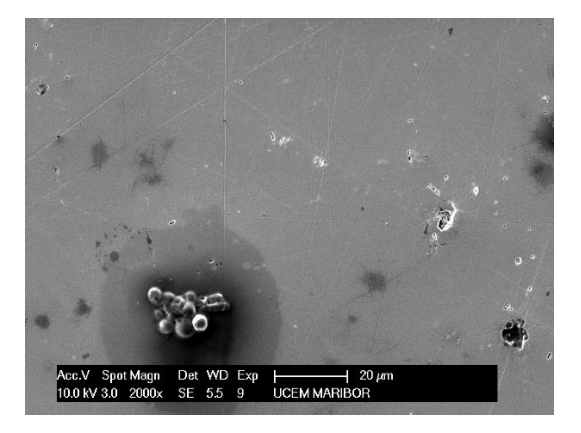
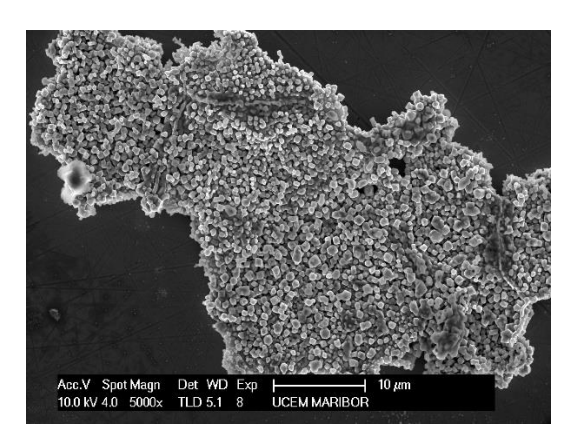


Figure 3. SEM images for AISI 347 at 75°C and pressure: a) 100 bar and b) 300 bar.



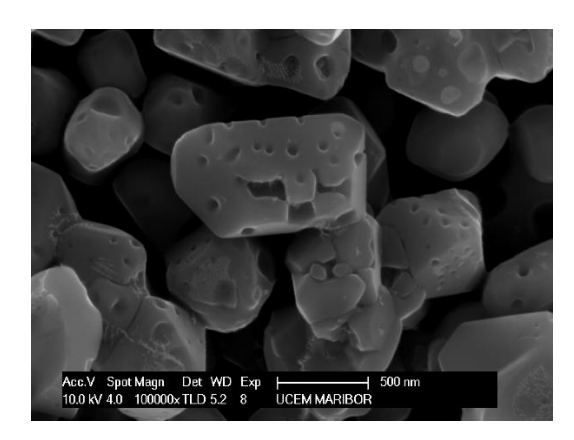


Figure 4. SEM images for AISI 347 at 75°C and 100 bar at different magnitudes.

At 75°C (Figures 3,4) and 100 bar some large structures of particles on the steel surface are visible. With EDS we detected high content of oxygen, iron and also chromium, in %: O 35.40, Fe 20.23 and Cr 41.82. Apparently, iron and chromium oxides precipitated and niobium accelerates their formation in the passive layer. A formation shown in Figure 3b (75°C at 300 bar) was identified as a carbide. The EDS analysis shows a high content of carbon, in %: C

29.18, O 12.85, Si 1.19, S 6.65, Cr 10.50, Fe 32.38, Ni 6.82 and Nb 0.43. In corrosion systems the carbides are always the worst option, as their formation leads to accelerated pitting corrosion.

3.2. Electrochemical impedance spectroscopy (EIS)

The passivity imposed on the system by the potential difference has values between Flade potential and transpassivity potential. The effect of this process can be deduced from the resistance values, which decrease at the Flade potential and remain low and almost constant, and then increase sharply in the area of transpassivity. With EIS the passive layer can be examined at any potential value. Impedance curves, which are measured during the corrosion process, lead to the construction of equivalent circuits, which illustrate and evaluate chemical processes on the examined material. ^{19, 33, 34}

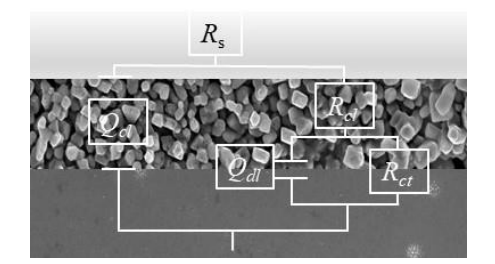


Figure 5. Equivalent circuit used for modelling the EIS results.

The RC equivalent circuit has been designed on the basis of the measured impedance curves shown in Fig. 5, where R_s represents the solution resistance, R_{cl} and R_{ct} the carbonate (pore) resistance and the charge transfer resistance, respectively. Q_{cl} and Q_{dl} are respectively Q of the carbonate (pore) and Q of double layer. Q is a frequency dependent element calculated from the CPE (constant phase element), which allows a better agreement between experimental and theoretical data.

The impedance of the CPE is defined: 19, 33

$$Z_{CPE} = [Q(j\omega)^{\alpha}]^{-1} \tag{1}$$

where Z is the electrode impedance, the frequency independent constant Q is a combination of properties related to the surface and the electroactive species, α is related to a slope of log Z vs. log f in the Bode plot, and is attributed to the surface heterogeneity, ω is the angular frequency.³⁵

The parameter Q (s^{α} Ω^{-1} cm⁻²) can be converted to the capacitance C (s Ω^{-1} cm⁻¹) at $\alpha < 1$ to quantitatively determine the system parameters, in particular the thickness, which is inversely proportional to the capacitance. When $\alpha = 1$, Q simply represents capacitance C.³⁶ Nyquist diagrams (Figures 6 and 7) show curves for samples treated at 1, 100 and 200 bar, which are typical for passive systems with high impedance values, and show two time constants, while the curves at 300 bar and untreated samples show classic semi-circular shapes. For the data collected for untreated steel and for sample at 50°C and 300 bar, only one time constant is visible in the impedance diagram. The HF part of the diagram can refer to the FeCO₃ layer or even to the mixture of FeCO₃ and F₃C carbide layers.³⁷

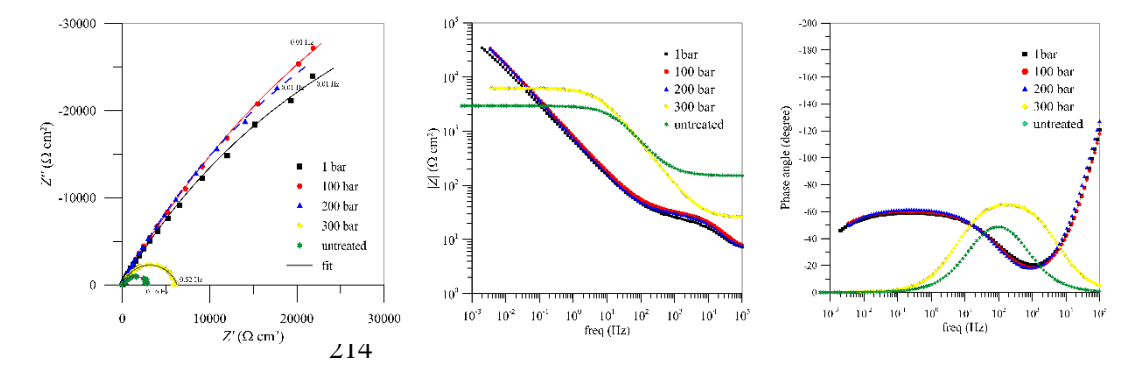


Figure 6. Impedance spectra for AISI 347 at 50°C: a) Nyquist plot, b) and c) Bode plot

The LF part corresponds to the charge transfer process. From Figures 6 and 7 it can be seen that the highest charge transfer resistance shows steel treated at 100 bar, lower, but still similar are the values for samples treated at 1 and 200 bar, while the R_{ct} value for the 300 bar sample decreases significantly, but is still slightly higher than for untreated steel.

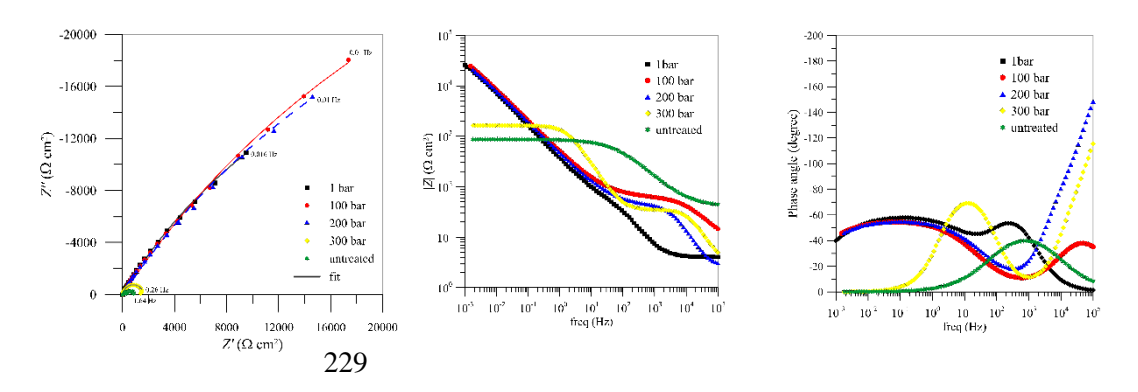


Figure 7. Impedance spectra for AISI 347 at 75°C: a) Nyquist plot, b) and c) Bode plot

Data from equivalent circuits are collected in Table 1.

Table 1. Parameter values from EIS measurements for AISI 347 at 50 and 75°C.

	P	$R_{ m po}$	$Q_c \cdot 10^{-6}$	α	$R_{\rm ct}$	Q_{dl} · 10^{-6}	α
	(bar)	(Ωcm^2)	$(s^{\alpha}\Omega^{-1}$		$(k\Omega cm^2)$	$(s^{\alpha}\Omega^{-1}cm^{-2})$	
			cm ⁻²)				
	1	34	8.40	0.71	120	440	0.67
	100	39	3.78	0.77	170	360	0.68
50°C	200	38	4.00	0.78	130	370	0.76
	300				6.20	9.20	0.80
	untreated				2.80	9.99	0.77
	1	60	93	0.80	68	750	0.65
	100	56.27	3.7	0.76	110	650	0.63
75°C	200	45	1.3	0.98	95	700	0.63
	300	38	0.46	0.98	1.6	67	0.95
	untreated				0.83	22.6	0.65

The comparison between the working temperatures is clear and to be expected: temperature accelerates corrosion, which is expressed in lower impedance values and lower R_{ct} values, Figure 8.

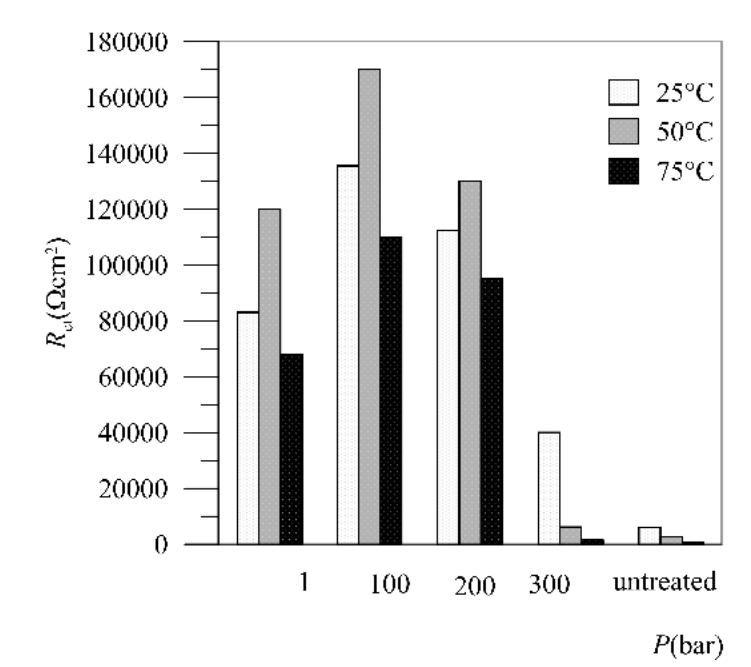


Figure 8. Calculated charge transfer resistance for AISI 347 at 25²⁹, 50 and 75°C depending on the pressure treatment.

3.3. Potentiodynamic polarization

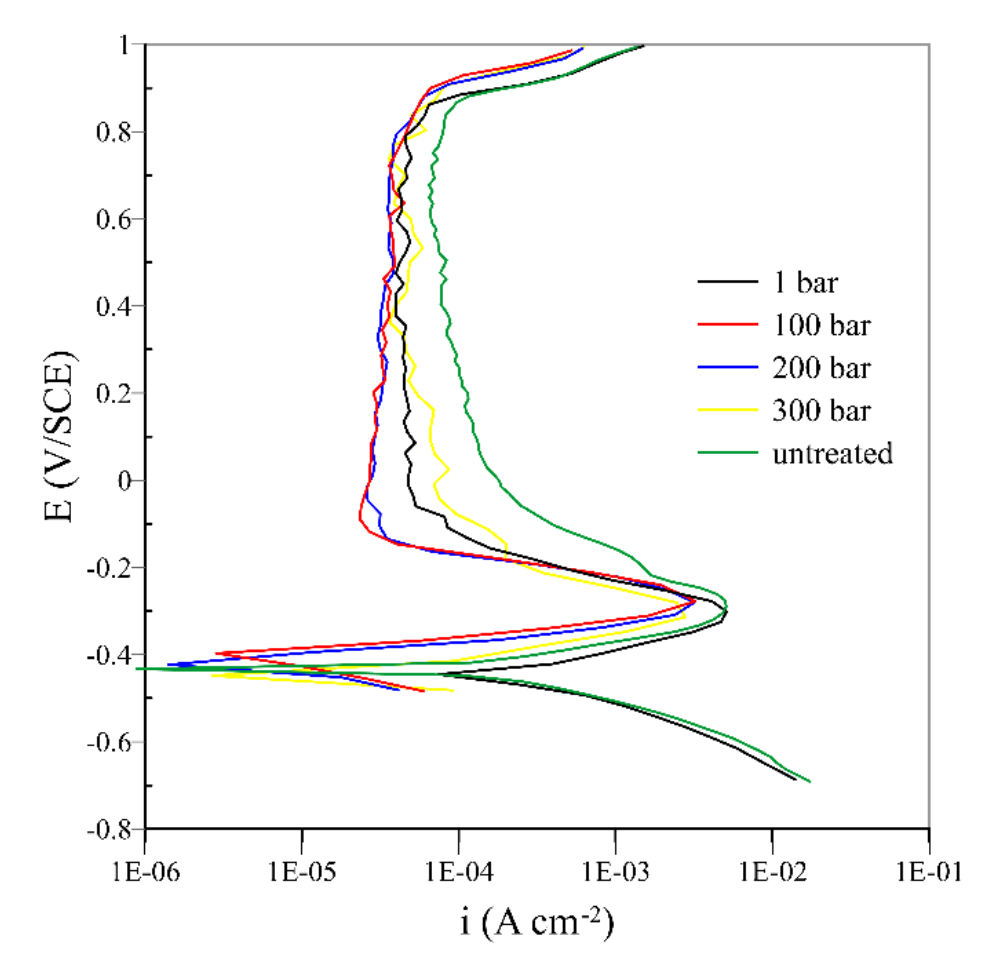


Figure 9. Polarization curves for AISI 347 at 50°C.

From polarization curves presented in Figure 9 (example at 50°C), the parameters listed in Table 2 were read out.

On the basis of Tafel extrapolation 38 from corrosion currents, i_{corr} , corrosion rates in mm per year were calculated, which are listed in Table 2 and also shown in Figure 10 including values for the corrosion rates at 25° C. 29 The E_{pas} values are the highest (shifted towards more positive values) for a sample treated at 100 bar, these samples also show the lowest i_{corr} , the largest passive range (E_{pas} - E_{trans}) and the lowest corrosion rates.

Table 2. Parameter values from potentiodynamic curves for AISI 347.

	P	<i>i</i> _{corr} ·10 ⁻⁵	<i>i</i> _{crit} ·10 ⁻³	E_{pas}	$E_{ m trans}$	$E_{ m pas}$ - $E_{ m trans}$	r_{corr}
	(bar)	(A cm ⁻²)	(A cm ⁻²)	(V/SCE)	(V/SCE)	(V/SCE)	$(mm y^{-1})$
50°C	1	1.680	2.80	-0.130	0.794	0.924	0.196
	100	0.821	3.53	-0.164	0.831	0.996	0.096
	200	1.174	3.36	-0.154	0.812	0.966	0.137
	300	9.372	2.89	-0.144	0.768	0.912	1.090
	untreated	13.05	5.10	-0.048	0.759	0.804	1.525
75°C	1	5.624	4.67	-0.171	0.739	0.910	0.657
	100	2.744	1.87	-0.175	0.748	0.924	0.320
	200	4.600	4.56	-0172	0.741	0.913	0.537
	300	15.24	1.33	-0164	0.738	0.902	1.780
	untreated	22.08	9.86	-0.013	0.731	0.744	2.581

bar.

From Figure 10, we can determine the best results for measured system at 50°C and 100

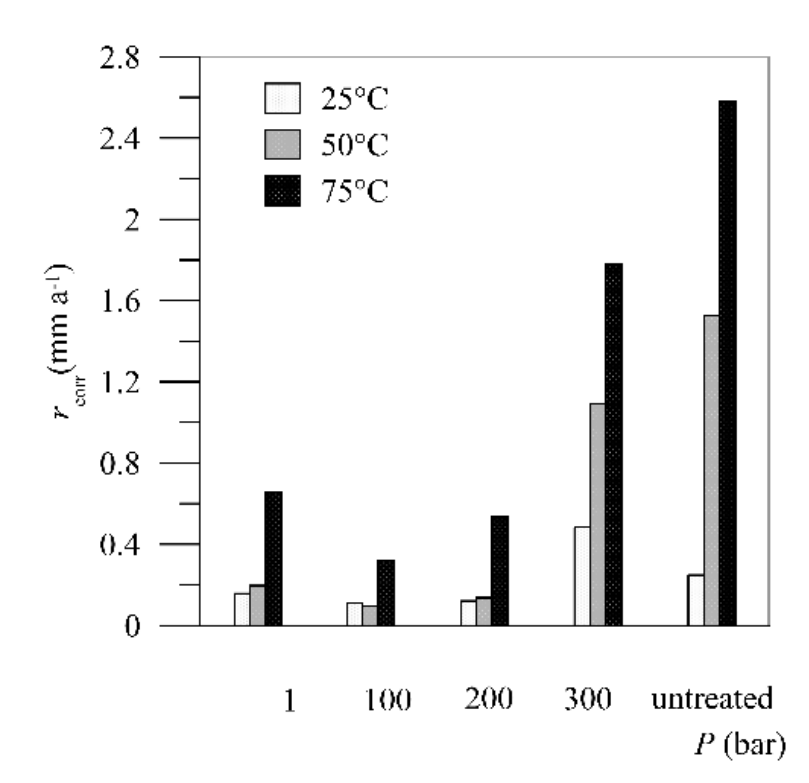


Figure 10. Corrosion rate for AISI 347 at 25²⁹, 50 and 75°C in dependence of pressure.

3.4. Activation energy calculation

The temperature dependence of the corrosion current density at different pressure values was further determined. Data at 25°C (published in earlier work²⁹), 50 and 75°C were considered. The values of the activation energy were calculated using the Arrhenius equation:³⁹, 40

$$\ln i_{\text{corr}} = \ln A - \frac{E_a}{RT}, \tag{2}$$

where A is pre-exponential factor, E_a is activation energy and R is a gas constant. Activation energy values are given in Figure 11.

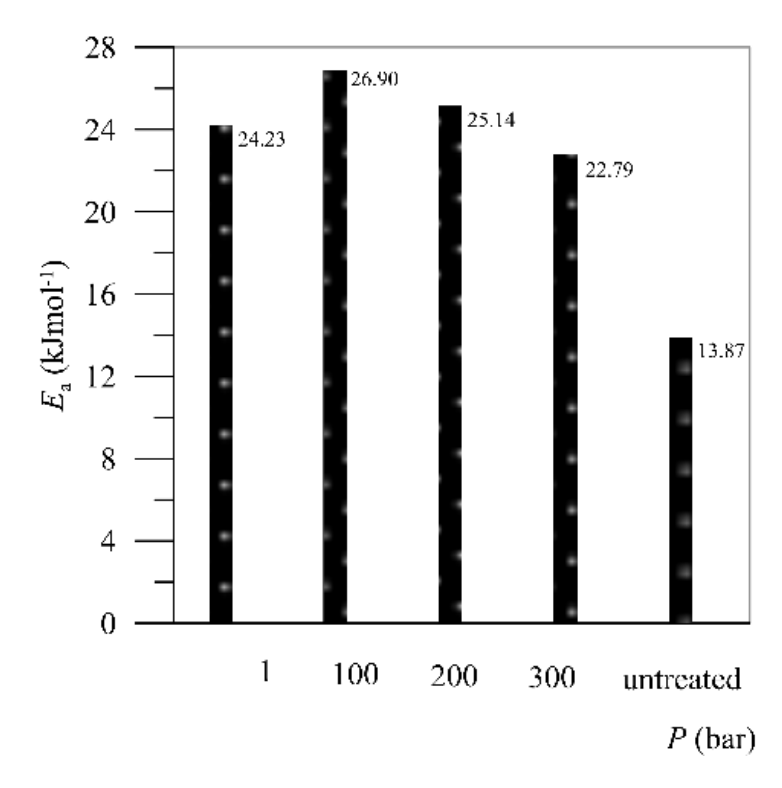


Figure 11. Activation energy values for AISI 347 in dependence of pressure treatment.

The activation energy represents the minimum energy that the reactants must have to form a product. In our case, the passive layer has already been formed, so that the activation energy can be related to the process of dissolving the layer. From the data obtained it can be concluded that the highest corrosion rate would be that of untreated steel, since the process of dissolution of the passive layer requires a minimum energy of 13.87 kJ/mol, unlike steel treated at 100 bar,

which has the highest value of activation energy of 26.9 kJ/mol and would therefore corrode at the lowest rate.

287

285

286

288

289 **4. Discussion**

290291

292

293

294

295

296

297

298

299

300

301

302

303

304

305

306

307

308

309

310

311

312

313

314

315

316

317

318

319

SEM images and in particular EDS analyses show that at 100 bar and 50°C treated steel (which indicates the best corrosion results) the content of oxygen embedded in the passive layer to build up protective compounds increases by up to 30 wt % determined on a dark, more or less uniformly corroded surface, without precipitants.

As the temperature rises to 50°C, the oxygen content increases considerably: from 2 to 9 wt.% and the carbon content increases from 1.1 to 2.3 wt.%. The oxygen content in precipitated white particles increases up to 43 wt.% (in relation to Fe - 15.8 wt.%, which clearly indicates the formation of FeCO₃, and the chromium content also increases up to 20 wt.%, (Figure 1a). By increasing the operating temperature to 75°C of the sample treated at 100 bar, the oxygen content decreases to 35 wt.% but at the same time increases the carbon content. For the sample treated at 300 bar, which indicates the highest corrosion rate between the treated samples, the EDS data are as follows: the oxygen content on the dark surface decreased from 24.7% at 50°C to 1.7% at 75°C. White precipitates, which are clearly visible in Figures 2b) and 3b), contain 41.4 wt.% oxygen at 50°C, which decreases to 8 wt.% at 75°C, while the carbon content increases from 0.46 wt.% to 9.5 wt.% as the temperature rises. A significant pressure increase obviously leads to an accelerated precipitation of carbon or carbon compounds. It is obvious that the corrosion behaviour at increasing pressure and temperature depends on the FeCO₃ precipitation mechanism. Choi et al. ⁴¹ found that the concentrations of CO₂, H₂CO₃ and HCO₃ in the water - CO₂ system for transport pipelines increase with increasing pressure but decrease with increasing temperature. The solubility of water in CO₂ reaches its almost lower value at 55°C (compared to 55 and 75°C) and 100 bar. It was also found that the reduced grain size of FeCO₃ forms a denser and therefore more efficient protective layer. These results are also in good agreement with our findings. The comparison between images a) and b) in Fig. 1 shows the small grain sizes that have grown at 100 bar compared to the large gain size at 300 bar, indicating slower layer growth at 300 bar, which leads to a porous layer and thus to a higher corrosion rate. Pfennig et al.³¹ also confirmed that the corrosion rates at 100 bar are lower compared to the ambient pressure, assuming that this could be due to an open capillary system within the corrosion layer that is not present in the high pressure system and thus prevents rapid mutual diffusion of the ionic species. We can assume that at 1 and 200 bar the mechanism of protective layer growth is the same as at 100 bar, as also indicated by Zhang et al.²⁵ (studied at 10 and 95 bar). One would expect the corrosion rate to decrease steadily with pressure, but at 300 bar it changes significantly. At high pressures, the amount of CO₂ dissolved in water and some other CO₂ properties should be considered, for example the compressibility factor.

The compressibility factor for CO₂, calculated with a modified Redlich-Kwong equation according to Spycher et at.⁴² and Lemmon at al.⁴³ showed the lowest value exactly between 100 and 200 bar at about 50°C compared to about 70°C. At 300 and up to 600 bar it increases linearly. At 100 bar, the value of the compressibility factor is about 0.38 compared to 300 bar, which indicates a value of 0.6, meaning that at 300 bar the CO₂ molecules collide more often and hardly move at all. This can explain the slower diffusion and thus the formation of a porous layer with large particles which consequently leads to a high corrosion rate.

5. Conclusions

In this study the corrosion behaviour of AISI 347 in 0.1 M sulphuric acid at temperatures of 50 and 75°C and pressures 1, 100, 200 and 300 bar in CO₂ atmosphere was investigated. An increased pressure significantly reduced the corrosion rate compared to untreated steel. The decisive points of our contribution are:

- A surface analysis was used to detect both the FeCO₃ layers and the precipitated grains, whose size varies according to the CO₂ pressure level.
- The corrosion rate determined by electrochemical methods decreases from 1 to 200 bar, is lowest at 100 bar, but increases significantly at 300 bar.
 - We attribute this sudden change to a compressibility factor of the CO₂, which allows us to explain the movement and collision of the molecules with each other, leading to their slower diffusion and consequently to the formation of a porous layer with large grains, which is noticeable as an increase in the corrosion rate.
- The best conditions for the lowest corrosion rate were found at 50°C and 100 bar. This combination shows the following results:
- A small grain size precipitates, causing them to adhere closely together, resulting in a denser and ticker protective layer of FeCO₃, which is therefore more resistant to further dissolution.
- Charge transfer resistance showed the highest value, which confirmed the lowest corrosion
 rate.

- The activation energy for dissolution of the protective layer showed the highest value,
- 354 confirming the best passivation.
- All conclusions are in good agreement with the value of the compressibility factor of CO₂
- at 100 bar, which allows us to explain the movements of its molecules on which the
- formation and the properties of the protective layer depend.

359

Acknowledgements

This work was supported by Slovenian Research Agency, grant P2-006.

361

362

363 **6. References**

- 1. A. Assarian, S. M., Improving Polyaspartic Anti-Corrosion Coating Protective Properties with the use of Nano-silica. *Acta Chim. Slov.* **2018**, *65*, 569 577.
- 367 2. Itman Filho, A.; Silva, R.; Cardoso, W.; Casteletti, L. C., Effect of Niobium in the Phase
- 368 Transformation and Corrosion Resistance of One Austenitic-ferritic Stainless Steel. Materials
- 369 *Research* **2014,** *17*, 801-806.
- 370 3. Gonzaga, A. C.; Barbosa, C.; Tavares, S. S. M.; Zeemann, A.; Payão, J. C., Influence of post
- welding heat treatments on sensitization of AISI 347 stainless steel welded joints. Journal of
- 372 *Materials Research and Technology* **2020**, *9* (1), 908-921.
- 4. Huang, S. Y.; Tsai, W.-T.; Pan, Y.-T.; Kuo, J.-C.; Chen, H.-W.; Lin, D.-Y., Effect of Niobium
- Addition on the High-Temperature Oxidation Behavior of 22Cr25NiWCoCu Stainless Steel in Air.
- 375 Metals Open Access Metallurgy Journal 2019, 9, 975.
- 5. Morks, M. F.; Corrigan, P.; Birbilis, N.; Cole, I. S., A green MnMgZn phosphate coating for steel
- pipelines transporting CO₂ rich fluids. Surface and Coatings Technology **2012**, 210, 183-189.
- 6. Morks, M. F.; Fahim, N. F.; Muster, T. H.; Cole, I. S., Cu-based Fe phosphate coating and its
- application in CO₂ pipelines. Surface and Coatings Technology **2013**, 228, 167-175.
- 7. Wang, Q.-Y.; Wang, X.-Z.; Luo, H.; Luo, J.-L., A study on corrosion behaviors of Ni–Cr–Mo laser
- coating, 316 stainless steel and X70 steel in simulated solutions with H2S and CO₂. Surface and
- 382 *Coatings Technology* **2016,** 291, 250-257.
- 8. Zhao, Y.; Liu, W.; Banthukul, W.; Fan, Y.; Li, X., Effect of silty sand on the pre-passivation
- behaviour of 1Cr steel in a CO₂ aqueous environment. Corrosion Engineering, Science and
- 385 *Technology* **2020**, *55* (3), 205-216.
- 9. Cen, H.; Cao, J.; Chen, Z.; Guo, X., 2-Mercaptobenzothiazole as a corrosion inhibitor for carbon
- steel in supercritical CO₂-H₂O condition. *Applied Surface Science* **2019**, 476, 422-434.

- 388 10. Zhang, H.-h.; Pang, X.; Gao, K., Localized CO₂ corrosion of carbon steel with different
- microstructures in brine solutions with an imidazoline-based inhibitor. Applied Surface Science
- **2018,** *44*2, 446-460.
- 391 11. Singh, A.; Lin, Y.; Ansari, K. R.; Quraishi, M. A.; Ebenso, E. E.; Chen, S.; Liu, W.,
- 392 Electrochemical and surface studies of some Porphines as corrosion inhibitor for J55 steel in sweet
- 393 corrosion environment. *Applied Surface Science* **2015**, *359*, 331-339.
- 394 12. López, D. A.; Pérez, T.; Simison, S. N., The influence of microstructure and chemical composition
- of carbon and low alloy steels in CO₂ corrosion. A state-of-the-art appraisal. *Materials & Design*
- **2003**, *24* (8), 561-575.
- 397 13. Dugstad, A., Fundamental Aspects of CO₂ Metal Loss Corrosion Part 1: Mechanism. NACE -
- 398 International Corrosion Conference Series **2006**, 2015.
- 399 14. A.Dugstad, The Importance of FeCO₃ Super-saturation on CO₂ Corrosion of Carbon Steels
- 400 CORROSION/1992, Paper No.14, (Houston, TX: NACE International, 1992)
- 401 15. A. Dugstad, H. H., M. Seiersten, Effect of Steel Microstructure on Corrosion Rate and Protective
- 402 Iron Carbonate Film Formation. *Corrosion* **2001**, *47* (4), 369 378.
- 403 16. Heuer, J. K.; Stubbins, J. F., An XPS characterization of FeCO₃ films from CO₂ corrosion.
- 404 *Corrosion Science* **1999**, *41* (7), 1231-1243.
- 405 17. Sun, W.; Nesic, S., Basics Revisited: Kinetics of Iron Carbonate Scale Precipitation in CO₂
- 406 Corrosion. In *CORROSION 2006*, NACE International: San Diego, California, 2006; p 21.
- 407 18. Yoon-Seok Choi, S. N., Corrosion Behavior Of Carbon Steel In Supercritical CO₂-Water
- 408 Environments. CORROSION 2009, 22-26 March, Atlanta, Georgia 2009.
- 409 19. Nešić, S.; Lee, K. L. J., A Mechanistic Model for Carbon Dioxide Corrosion of Mild Steel in the
- 410 Presence of Protective Iron Carbonate Films—Part 3: Film Growth Model. *Corrosion* **2003**, *59* (7),
- 411 616-628.
- 412 20. Sun, W.; Nešić, S.; Woollam, R. C., The effect of temperature and ionic strength on iron carbonate
- 413 (FeCO₃) solubility limit. *Corrosion Science* **2009**, *51* (6), 1273-1276.
- 21. Nešić, S., Key issues related to modelling of internal corrosion of oil and gas pipelines A review.
- 415 *Corrosion Science* **2007**, *49* (12), 4308-4338.
- 416 22. C. DE WAARD, D. E. M., Carbonic Acid Corrosion of Steel. *CORROSION* **1975**, *31* (5), 177-181.
- 417 23. Srdjan Nešić, S. W., Keith George, High Pressure CO₂ Corrosion Electrochemistry and the Effect
- 418 of Acetic Acid. CORROSION 2004, 28 March-1 April, New Orleans, Louisiana 2004.
- 419 24. Sun, Y.; Nesic, S., A parametric study and modeling on localized CO₂ corrosion in horizontal wet
- gas flow. NACE Meeting Papers 2004.
- 421 25. Zhang, Y.; Pang, X.; Qu, S.; Li, X.; Gao, K., Discussion of the CO₂ corrosion mechanism between
- low partial pressure and supercritical condition. *Corrosion Science* **2012**, *59*, 186-197.
- 423 26. Li, X.; Zhao, Y.; Qi, W.; Xie, J.; Wang, J.; Liu, B.; Zeng, G.; Zhang, T.; Wang, F., Effect of
- 424 extremely aggressive environment on the nature of corrosion scales of HP-13Cr stainless steel.
- 425 Applied Surface Science **2019**, 469, 146-161.

- 426 27. Wang, Z. M.; Han, X.; Zhang, J.; Wang, Z. L., In situ observation of CO₂ corrosion under high
- pressure. *Corrosion Engineering*, *Science and Technology* **2014**, 49 (5), 352-356.
- 428 28. Milošev, I., Contemporary Modes of Corrosion Protection and Functionalization of Materials. Acta
- 429 *Chim. Slov.* **2019,** *66*, 511-533.
- 430 29. M. Slemnik; Pečar, D., High-pressure CO₂ pretreatment as a method for stainless steel passivation.
- 431 *Anti-Corrosion Methods and Materials* **2010**, *57* (6), 290 296.
- 30. ZView, ZPlot, CorrView, CorrWare, version 2.8. Scribner Associates, Inc, Southern Pines, NCD,
- 433 *USA* **1990-1999**.
- 434 31. Pfennig, A.; Kranzmann, A., Effect of CO₂ and pressure on the stability of steels with different
- amounts of chromium in saline water. *Corrosion Science* **2012**, *65*, 441-452.
- 436 32. A. Pfennig, A. K., The Role Of Pit Corrosion In Engineering The Carbon Storage Site At Ketzin,
- Germany. WIT Transactions on Ecology and the Environment **2010**, 136, 109-119.
- 438 33. A.S. Hamdy; E. El-Shenawy; El-Bitar, T., Electrochemical Impedance spectroscopy of the
- corrosion behaviour of some niobium bearing stainless steels in 3.5% NaCl. *International Journal*
- 440 *of Electrochemical Science* **2006,** *Vol.1*, 171-180.
- 441 34. Tan, Z.; Yang, L.; Zhang, D.; Wang, Z.; Cheng, F.; Zhang, M.; Jin, Y., Development mechanism
- of internal local corrosion of X80 pipeline steel. Journal of Materials Science & Technology 2020,
- 443 49, 186-201.
- 444 35. Mark E. Orazem, I. F., Bernard Tribollet, Vincent Vivier,; Sabrina Marcelin, N. P., Annette L.
- Bunge, Erick A.White,; Musianif, D. P. R. a. M., Dielectric Properties of Materials Showing
- 446 Constant-Phase-Element (CPE) Impedance Response. Journal of The Electrochemical Society
- **2013,** *160* (6), C215 C225.
- 448 36. Hirschorn, B.; Orazem, M. E.; Tribollet, B.; Vivier, V.; Frateur, I.; Musiani, M., Determination
- of effective capacitance and film thickness from constant-phase-element parameters.
- 450 *Electrochimica Acta* **2010,** *55* (21), 6218-6227.
- 451 37. Farelas, F.; Galicia, M.; Brown, B.; Nesic, S.; Castaneda, H., Evolution of dissolution processes
- at the interface of carbon steel corroding in a CO₂ environment studied by EIS. Corrosion Science
- **2010,** *52* (2), 509-517.
- 454 38. Corrosion: Third Edition. Shreir, L. L.; Jarman, R. A.; Burstein, G. T., Eds. 1994; Vol. 1, pp 1-
- 455 2815.
- 456 39. P. W. Atkins, J. d. P., *Physical Chermistry*. Eight ed.; Oxford University Press Oxford, USA, 2006.
- 457 40. F. Mohammadinejad, S. M. A. H., M. S. Zandi, M. J. Bahrami, Z. Golshani, Metoprolol: New and
- Efficient Corrosion Inhibitor for Mild Steel in Hydrochloric and Sulfuric Acid Solutions. *Acta Chim.*
- 459 *Slov.* **2020,** *67*, 710-719.
- 460 41. Choi, Y.-S.; Nešić, S., Determining the corrosive potential of CO₂ transport pipeline in high p_{CO2}-
- 461 water environments. International Journal of Greenhouse Gas Control 2011, 5 (4), 788-797.

- 42. Spycher, N.; Pruess, K.; Ennis-King, J., CO₂-H₂O mixtures in the geological sequestration of CO₂.
- I. Assessment and calculation of mutual solubilities from 12 to 100°C and up to 600 bar.
- 464 *Geochimica et Cosmochimica Acta* **2003**, 67 (16), 3015-3031.
- 465 43. Lemmon, E. W.; McLinden, M. O.; Friend, D. G.; National Institute of S.; Technology,
- Thermophysical properties of fluid systems. **1998**.

468 Povzetek

S površinsko analizo in elektrokemijskimi metodami smo proučevali korozijske lastnosti jekla AISI 347 v 0,1 M raztopini žveplove kisline. Jeklo smo izpostavili CO₂ atmosferi pri povišani temperaturi in tlakih vse do 300 barov. Prisotnost CO₂ pospešuje nastanek zaščitne plasti iz FeCO₃, vendar je uspešnost takšnega pasiviranja odvisna od njegove nasičenosti in ustrezne temperature. Ne samo podobni, celo boljši rezultati so bili doseženi pri nižjih temperaturah s povišanjem tlaka. Razlike v korozijski hitrosti med vzorci smo potrdili tudi z določitvijo vrednosti aktivacijskih energij, ki jih sistem potrebuje za nadaljnje raztapljanje zaščitne plasti. Predpostavimo lahko, da stisljivost CO₂ pri različnih tlakih vpliva na poroznost zaščitne plasti železovega karbonata in posledično njenih korozijskih lastnosti.